



## Automated occlusion detection for the diagnosis of acute ischemic stroke: A detailed performance review

Freda Werdiger<sup>a,b,\*</sup>, Sunay Gotla<sup>e</sup>, Milanka Visser<sup>a,b</sup>, James Kolacz<sup>a,b</sup>, Vignan Yogendrakumar<sup>a,b</sup>, James Beharry<sup>a</sup>, Michael Valente<sup>a,b</sup>, Angelos Sharobeam<sup>a,b</sup>, Mark W. Parsons<sup>c,d,f</sup>, Andrew Bivard<sup>a,b</sup>

<sup>a</sup> Melbourne Brain Centre at Royal Melbourne Hospital, Melbourne, Australia

<sup>b</sup> Department of Medicine, University of Melbourne, Melbourne, Australia

<sup>c</sup> Apollo Medical Imaging, Melbourne, Australia

<sup>d</sup> Ingham Institute for Applied Medical Research, Liverpool, NSW, Australia

<sup>e</sup> Southwestern Sydney Clinical School, University of New South Wales, Sydney, Australia

<sup>f</sup> Department of Neurology, Liverpool Hospital, NSW, Australia

### ARTICLE INFO

#### Keywords:

Clot detection algorithm  
Acute ischemic stroke  
Perfusion imaging

### ABSTRACT

**Introduction:** Stroke is a leading cause of adult disability and death worldwide. Automated detection of stroke on brain imaging has promise in a time critical environment. We present a method for the automated detection of intracranial occlusions on dynamic CT Angiography (CTA) causing acute ischemic stroke.

**Methods:** We derived dynamic CTA images from CT Perfusion (CTP) data and utilised advanced image processing to enhance and display major cerebral blood vessels for symmetry analysis. We reviewed the performance of the algorithm on a cohort of 207 patients from the International Stroke Perfusion Imaging Registry (INSPIRE), with Large Vessel Occlusion (LVO) and non-LVO strokes. Included in the data were images with chronic stroke, various artefacts, incomplete vessel occlusions, and images of poorer quality. All images were annotated by stroke experts. In addition, each image was graded in terms of the difficulty of the task of occlusion detection. Performance was evaluated on the overall cohort, and with respect to occlusion location, collateral grade, and task difficulty. We also evaluated the impact of including additional perfusion data.

**Results:** Images with a rating of lower difficulty achieved a sensitivity and specificity of 96% and 90%, respectively, while images with a moderate difficulty rating achieved 88% and 50%, respectively. For cases of high difficulty, where more than two experts or additional data were required to reach consensus, sensitivity and specificity was 53% and 11%. The addition of perfusion data to the dCTA images increased the specificity by 38%.

**Conclusion:** We have provided an unbiased interpretation of algorithm performance. Further developments include generalising to conventional CTA and employing the algorithm in a clinical setting for prospective studies.

### 1. Introduction

Modern brain imaging has led to considerable advances in patient assessment for acute ischemic stroke. Imaging assessment of tissue pathophysiology has been instrumental in predicting tissue and clinical response to treatment [1]. Computed tomography perfusion (CTP) imaging is now widely used to estimate the volume of salvageable brain tissue that may be targeted by reperfusion therapies [2–5]. Although

endovascular clot retrieval (ECR) was initially limited to a benefit within six hours of stroke onset, CTP patient selection has subsequently shown a benefit up to 24 hours [6–8].

Selection of patients for thrombectomy relies on the identification of a retrievable thrombus on either angiography or non-contrast CT (NCCT). There have been numerous efforts to automate occlusion detection in order to facilitate the early identification of patients requiring thrombectomy in centres without imaging expert assessment.

\* Corresponding author at: Melbourne Brain Centre at Royal Melbourne Hospital, Melbourne, Australia.

E-mail address: [freda.werdiger@unimelb.edu.au](mailto:freda.werdiger@unimelb.edu.au) (F. Werdiger).

<https://doi.org/10.1016/j.ejrad.2023.110845>

Received 28 October 2022; Received in revised form 15 April 2023; Accepted 20 April 2023

Available online 25 April 2023

0720-048X/© 2023 Published by Elsevier B.V.

Prior studies e.g., [9] have prioritised the detection of large vessel occlusions (LVOs) over occlusions of more distal, smaller vessels. In this prior study [9], where 217 subjects were included overall, positive cases were restricted to a definition of LVO (intracranial occlusions of the internal carotid artery (ICA) and the M1 segment of the middle cerebral artery (M1-MCA)), and performance was reported with high sensitivity and specificity. While LVOs are often the most disabling strokes, they constitute only 15% of all cases that present at hospitals or clinics. Another study [10] tested an occlusion detection algorithm on two different datasets, one with 1110 patients and another with 646 patients, with ICA, M1-MCA and M2-MCA patients present in both datasets. Performance varied significantly between the two datasets, making it challenging to judge overall performance.

There is major clinical importance in detecting non-LVO occlusions, as such patients are still eligible for reperfusion therapy. While occlusions of the peripheral segments are expected to result in a smaller infarct volume, when they affect an eloquent region, they can cause significant clinical and functional impairment [11]. It is therefore valuable to achieve accuracy across different locations. Even while non-LVOs generally represent a lesser threat than LVOs, they still represent a therapeutic dilemma. In the case of M2 and M3 occlusions, the decision to offer reperfusion therapy (e.g., IV lysis versus endovascular occlusions retrieval versus no reperfusion therapy) is more complex than in M1 and ICA occlusions, and computational assistance may therefore prove more useful in those cases than with LVOs, where the decision is less controversial. Indeed, it has been estimated that 54% of M2 patients achieve a good functional outcome without treatment [12]. However, occlusions of more distal, smaller vessels are often difficult to detect, particularly for less expert clinicians [13]. An occlusion detection tool that succeeds with difficult or complex cases would be useful in environments without a specialist stroke neurologist or neuroradiologist; such sites include nearly all rural and regional hospitals [14].

Within the LVO population, there is also some challenge in detecting occlusions that are incomplete (i.e., where the vessel lumen is not totally occluded and there is still some antegrade flow), or occlusion sites where robust collateral flow effectively supplies the occluded vessel's territory distal to the occlusion [15]. Prior automated occlusion detection studies have not included data where there is patient motion, more distal or complex occlusions, or partial (incomplete) occlusions. As such, the occlusion detection results in prior studies are not generalisable to everyday clinical practice.

In the present study we sought to use a more representative, clinical cohort that may be generalisable to real-world scenarios to develop and validate a new occlusion detection algorithm with the aim of improving the reliable occlusion detection in patients with a suspected acute ischemic stroke.

## 2. Methods

### 2.1. Dataset

We included retrospective data from 209 patients that were previously recruited from two different comprehensive stroke centres between 2010 and 2020. All patients included in this study had been prospectively enrolled as part of the International Stroke Perfusion Imaging Registry (INSPIRE). INSPIRE was approved by the Hunter New England Local Health District Human Research Ethics Committee in accordance with Australian National Health and Medical Research Council guidelines (Reference No. 11/08/17/4.01). All INSPIRE patients were recruited at participating stroke centres. An opt-in consent approach was initially used (requiring subjects to submit a form of consent) and was later changed to an opt-out consent approach under new government policy. This required subjects to submit a form if they wish to be removed from the INSPIRE database. All data is de-identified and not re-identifiable. Data from this study will be shared at the request of other researchers via an institutional email address made to the

corresponding author in a reasonable timeframe.

Inclusion criteria was as follows: All patients presented to one of the two stroke centres under suspicion of acute ischemic stroke and underwent diagnostic CTP imaging. Any datasets with missing data were not included. High resolution, complete, datasets were selected from INSPIRE based on the physical spacing between pixels (less and or equal to 1 mm) and the amount of physical coverage (total brain). At this stage of development, under these criteria, only data from the Toshiba Aquilion ONE scanner (Toshiba Medical Systems; Tokyo, Japan) was available to include.

### 2.2. Image acquisition

All patients underwent whole brain CTP imaging with the Toshiba Aquilion scanner. Nineteen time points were acquired over 60 s for CTP imaging. The image acquisition commenced seven seconds after the initiation of 40 mL contrast injection at 6 mL/s (Ultravist 370 Bayer HealthCare; Berlin, Germany). Images were acquired across two separate sites, both comprehensive stroke centres. Two patient datasets were excluded due to severe noise artefact; Two patient datasets were annotated but later discarded due to failed registration to a template (see Appendix A).

Site 1 (n = 115): The perfusion image acquisition consisted of three phases: the first phase was a one frame baseline image (80 kV, 310 mA); the second phase started at three seconds and acquired 13-time points (80 kV, 150/300 mA) with two second intervals; the third phase started at 40 s and acquired five time points (80 kV, 150 mA) with five second intervals. One gantry rotation time was 0.75 s, and it resulted in 320 axial slices with 0.5 mm thickness. Field of view (FOV) was 220 × 220 mm and matrix size was 512 × 512.

Site 2 (n = 94): The perfusion image acquisition consisted of three phases: the first phase was a one frame baseline image (80 kV, 310 mA); the second phase started at three seconds and acquired 13 time points (80 kV, 150/300 mA) with two second intervals; the third phase started at 40 s and acquired five time points (80 kV, 150 mA) with five second intervals. One gantry rotation time was 0.75 s, and it resulted in 160 or 180 axial slices with 0.5–1 mm thickness. Field of view (FOV) was 220 × 220 mm and matrix size was 512 × 512.

Raw CTP DICOM (Digital Imaging and Communications in Medicine) data was processed using MISTar (Apollo Medical Imaging, Melbourne, Australia). Dynamic CT Angiography (CTA) data was derived from the raw CTP data. The algorithm performed motion correction and discarded any acquisition points with severe motion artefacts. The arterial phase of the CTP acquisition protocol was the time points corresponding to the first peak in contrast, as determined by the Arterial Input Function (AIF). The mean arterial phase was the mean of all peak arterial phase time frames (usually two or three frames). This was calculated automatically for each patient dataset. An example is shown in Fig. 1. Maps of cerebral perfusion were also processed via MISTar on the same dataset and were used by the raters to assist in locating the occlusion, and by the algorithm to assist in detecting occlusions.

### 2.3. Expert annotations

All images were reviewed by a team of four expert stroke neurologists with 6 or more years of stroke and neurology training (AS, JB, MV, VY). Readers were presented with fully anonymized images in a Neuroimaging Informatics Technology Initiative (NifTI) format, along with the age and sex of each patient, and instructed to interpret cases approximating clinical practice as closely as achievable. All readers used ITK-SNAP (compatibility version 3.4.10) [16] to view the images, able to adjust intensity values (windowing) to view vessels in high contrast, and to scroll through slices in all axes. In addition, perfusion data was supplied to the readers. The perfusion data could be viewed alone in ITK-SNAP or overlaid directly on the patient CTA. Perfusion data showed the presence of a perfusion lesion as calculated by MISTar. For each

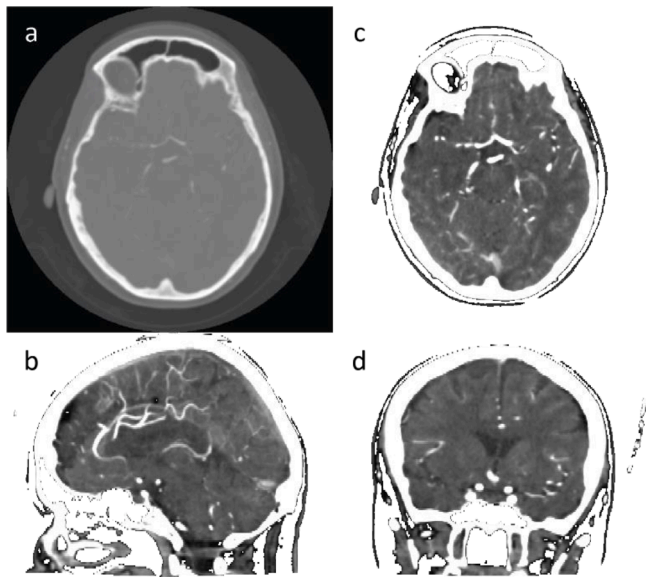


**Fig. 1.** Mean arterial phase image. An axial slice shown in (a); slices (displayed image intensity is limited (windowed) to between 0 and 200 Hounsfield units to highlight soft tissue and the vessel contrast agent) of the axial, sagittal and coronal planes are shown in (b), (c) and (d), respectively, to display vessels more clearly.

patient dataset, two readers reviewed the images together (either AS or VY, or JB and MV), only providing an annotation once an agreement was made. If there was no consensus, an independent reviewer (senior stroke neurologist, MP) was called in to adjudicate. For each image, the following consensus information was recorded: occlusion presence (yes:  $n = 164$ ; no:  $n = 43$ ), occlusion location (ICA; 8, M1-MCA; 82, M2-MCA; 48, M3-MCA; 7, ACA; 4, PCA; 9 and Basilar; 6), occlusion hemisphere (right; 75, left; 83) and quality of collateral flow (good; 43, moderate; 74 and poor; 47).

Three patients had occlusions that were not visible within the imaged volume, e.g., extracranial or proximal ICA, and were marked as having no visible occlusion. Seven patients had also suffered a previous stroke which was visible on the CT image. Of these seven patients, six patients were suffering from an acute ischemic stroke at the time of imaging, and one was not. None were excluded as they represented real-world diagnostic scenarios. Evaluation on these cases were necessary to gauge real-world performance.

#### 2.4. Algorithm process

**Fig. 2** outlines the process graphically. Each step is described below, with reference to each stage shown in **Fig. 2**. Further detail found in **Appendix A** such that the process may be reproduced.

(a) **Registration to template.** Mean arterial phase images were registered to a publicly available template using the Advanced Normalization Toolkit (ANTs) [17,18] and skull stripping was performed; (b) **Vessel enhancement.** A Hessian-based vesselness filter was applied using the Insight Toolkit [19], highlighting vessel-like objects only; (c) **Sliding Maximum Intensity Projection (MIP) image.** Using the output of the vesselness filter, a novel MIP image was created, which we call a Sliding MIP. Exact details on how to create this image is shown in **Appendix A**. The effect, seen in **Fig. 2**, created a clear picture of vessel from which the location of the occlusion can be visually identified; (d) **Difference map.** A difference map was created by flipping the sliding MIP around the vertical axis and subtracting the original image from the flipped image. This was done to enhance the site of any difference in contrast between hemispheres that may indicate a deficit of contrast in vessels on one side; (e) **Seeds.** Connected Component Labelling (CCL) was performed on the

difference map using ITK. The function of CCL is to assign a unique label to all pixels that form part of a connected component. Each connected component was treated as the potential site of a deficit and called a 'seed'. All detail on this step is given in **Appendix A** for reproducibility; (f) **Ranking.** All seeds were given a score based on size, location, and severity (the amplitude of the difference between sides). Details on how these were quantified is in **Appendix A**; (g) **Perfusion.** If the perfusion data was available, it was only used as follows: A seed was required to lie in the same hemisphere as a perfusion lesion. If a seed was in a difference hemisphere, it was discarded; (h) **Coronals.** Step (c) was repeated to create a Sliding MIP in the coronal plane. Steps (d) – (g) were then repeated for deficits in the coronal plane. If a detection in the axial plane lay at the same position as the coronal plane, an occlusion detection was made.

#### 2.5. Performance evaluation

Each image was marked upon visual inspection by a clinical expert (MP) with a true positive (TP), false positive (FP), true negative (TN) or false negative (FN). If the ranking seed that was selected coincided with the correct occlusion position or the perfusion deficit that was a *direct result* of the occlusion, a TP was assigned. If an occlusion was present but the detection was too far from the occlusion site to be considered a TP, a FP was assigned.

The performance of the algorithm was measured using sensitivity, specificity, positive predictive value (PPV), negative predictive value (NPV), diagnostic odds ratio and accuracy. Where possible, confidence intervals (95%) were calculated using a bootstrap method, by randomly sampling the dataset and calculating each metric for each sample. A sample size of 50 was used and sampling was performed 1000 times. Performance was also evaluated over subsets of the data, measuring performance of datasets that are homogeneous with respect to occlusion location (ICA, M1, M2 and M3) and collateral flow (good/moderate/poor). Confidence intervals were not calculated for data subsets due to the relatively small sample sizes. The impact of adding perfusion data to the algorithm was also evaluated. In the event of a false positive detection, it was determined whether the detection correlated with the presence of a perfusion lesion either from a chronic stroke, or occlusion that was not within the image field-of-view (FOV). In addition, the algorithm was evaluated with respect to the difficulty of each case (low, moderate, and high difficulty). It is well known that larger vessel occlusions are more easily detected than occlusions of smaller vessels. Moreover, patients with robust collateral flow, or partial occlusions with residual antegrade flow and reconstitution of blood flow immediately distal to the occlusion presented a difficult challenge for detection. Therefore, each patient was categorized according to the difficulty of the case presented. Labels were designated by expert human raters as presenting a low, moderate, or high degree of difficulty in occlusion detection. Cases of low difficulty consisted of LVOs with abrupt cut-off and no residual flow, cases of high difficulty were such that more than two experts, or additional information, was required to locate the occlusion. Cases of moderate difficult did not require any additional information by the experts to locate but were less detectable than abrupt cut-off LVOs due to well-known reasons such as a more distal position, residual flow through the occlusion, or anatomical variation. Examples of each are shown in **Fig. 3**.

### 3. Results

#### 3.1. Dataset characteristics

Of the total study population, 99 (48%) were females. The median age was 72 (IQR 63–80) and the median baseline National Institutes of Health Stroke Scale (NIHSS) was 12 (IQR 6–18). The time of stroke onset was known for 165 (79%) of patients, and the median time between stroke onset and CTP imaging for these patients was 114 min (IQR 89 –

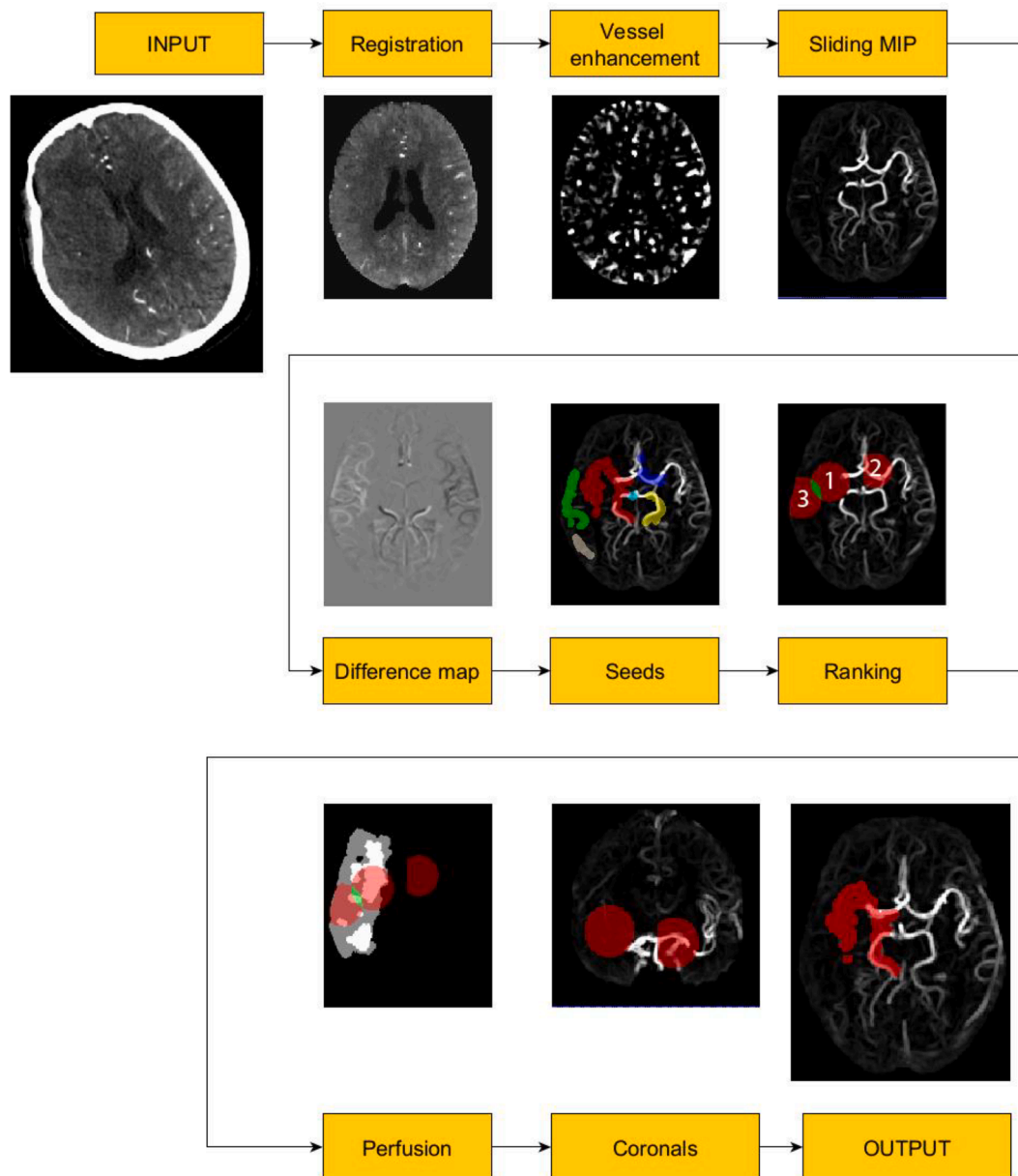


**Fig. 2.** Schematic of the algorithm process. This patient had an occlusion of the right M1 branch of the Middle Cerebral Artery; there is an abrupt vessel cut off with no residual flow. The raw image was registered to template and processed using a ‘vesselness’ filter. The Sliding Maximum Intensity Projection (MIP) highlighted deficit areas – shown here in a single slice. Left-right subtraction was used to identify areas where there are differences between hemispheres. Connected Component Labelling (CCL) was used to form “seeds”, shown in different colours. (In this case, a region corresponding to the right Posterior Cerebral Artery (PCA) was joined by CCL to the region corresponding to the deficit in the right M1-MCA due to their proximity). Each area received a ranking, with the areas of greatest concern receiving the highest ranking. Perfusion data (if available) was then used to confirm the detection. The process was then repeated in the coronal plane to ensure that a detection was present in both perspectives. Details of each step can be found in the main text with additional information in Appendix A.

166 min). For the remainder 20 patients (10%) were reported as ‘Wake-Up Stroke’ and 24 (11%) had an unknown time of stroke onset. Of the study population, 75 (36%) were treated with IV thrombolysis, 55 (26%) underwent endovascular (or intra-arterial – IA) therapy, and 38 (18%) received both therapies. Of the patients that received IV alone, two patients were planned to undergo IA therapy, but it was not delivered. Forty patients (19%) received no treatment for revascularization and one patient’s treatment was not documented. **Table 1** shows the occlusion characteristics for each level of difficulty, and overall.

### 3.2. Performance evaluation outcome

**Fig. 4** shows examples of successful occlusion detections. Further

results are shown in **Appendix B**.

**Fig. 5** shows two results from patients with occlusions close to the midline. The first example (labelled 1 in **Fig. 5**) is of a basilar occlusion. The analysis of left–right difference via CCL revealed the site of a contrast deficit associated with this occlusion, leading to a false positive. The second example (labelled 2 in **Fig. 5**) shows an ACA occlusion. Two axial slices are shown. While CCL return several potential regions, upon analysis, none were selected as a final detection.

**Table 2** shows results of the occlusion detection algorithm. From twenty-five False Positive results, thirteen coincided with the presence of a perfusion lesion. One of these was due to the presence of an occlusion that was not within the image slab (proximal ICA), and another was due to the presence of an old stroke. For the remaining two

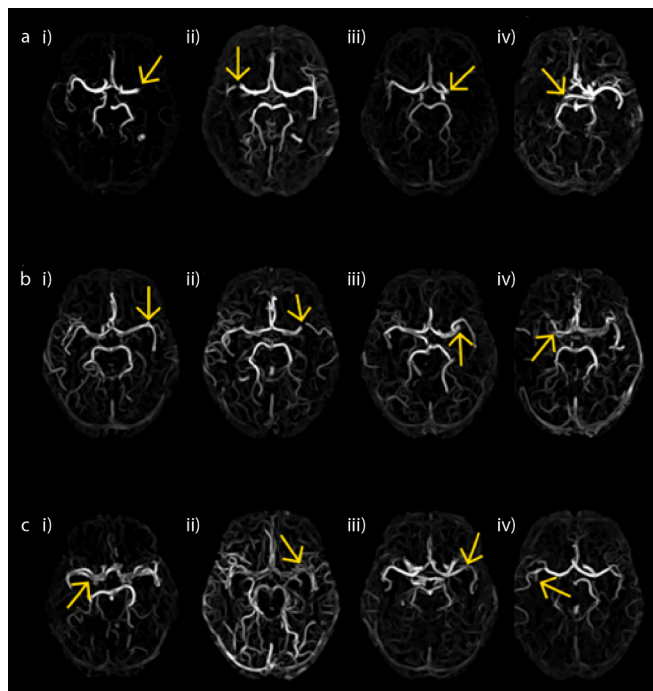


**Fig. 3.** Examples of Low, moderate and high levels of difficulty in images. Fig a) (low difficulty); (i) - (iii) are slices from M1 occlusions (with the occlusion in ii tapering off) and (iv) represents an occlusion in the internal carotid artery (outside the FOV). Fig b) (moderate difficulty); Both (i) and (ii) are M2 occlusions, (iii) is an image of an M1 occlusion with anatomical variation (early branching) so that one M2 branch has flow, and iv is an M1 occlusion with residual flow and reconstitution of flow distal to the occlusion. Fig c) (high difficulty); (i), (ii), (iii) and (iv) are all partial occlusions that were difficult for expert raters to see as there is reconstitution of vessel distal to the occlusion due to residual antegrade flow.

**Table 1**

Occlusion characteristics for patients overall, and for each category of difficulty, decided on by consensus among the expert raters.

Difficulty rating	All = 207	Low = 106	Moderate = 45	High = 56
No visible occlusion	43	30	6	7
ICA	8	8	0	0
MCA-M1	82	67	9	6
MCA-M2	48	1	29	18
MCA-M3	7	0	0	7
ACA	4	0	0	4
PCA	9	0	1	8
Basilar	6	0	0	6
Good Collaterals	43	15	11	17
Moderate Collaterals	74	27	20	27
Poor Collaterals	47	34	8	5

extracranial occlusions, both were not visualised by the algorithm. [Table 3](#) shows the results when perfusion data was not available. In summary adding perfusion lesion data to the algorithm increased specificity by 38% overall, albeit reducing sensitivity by 8%. [Table 4](#) shows the prevalence of occlusion types in the dataset and in the INSPIRE registry, overall. INSPIRE consists of consecutively enrolled acute ischemic stroke patients, prospectively recruited at comprehensive stroke centres.

When perfusion data was included, for cases of low difficulty, the sensitivity and specificity were 96% and 90%, respectively. For moderately difficult cases, specificity reduced to 50%. For cases with a high difficulty rating - many of which required consensus of an additional expert and/or perfusion data to confirm - the algorithm achieved a sensitivity of 53% and a specificity of 11%. On the entire cohort, a

sensitivity of 83% and specificity of 58% was achieved.

Performance metrics were evaluated over other subsets of data. Images of patients with poor collateral flow returned a sensitivity of 95%, better than those with robust collaterals: 78%. Specificity values were similar at 73% for poor and 76% for good collaterals. Sensitivity for datasets with M1 and M2 occlusions were 94% and 81%, respectively and specificity were 80% and 65%, respectively.

In addition, performance was evaluated for each site. For Site 1 (112 patients analysed), sensitivity and specificity were 89% and 68%, respectively. For Site 2 (93 patients analysed), sensitivity and specificity were 77% and 43%, respectively.

#### 4. Discussion

We have presented the method and results of a high sensitivity occlusion detection algorithm that may be applied to whole-brain contrast-enhanced time series perfusion CT images. We have evaluated the algorithm in a thorough manner which we believe better reflects real-world performance (and the heterogeneity of stroke pathophysiology) compared to other studies. For images of low difficulty (which past studies have restricted themselves to), the algorithm presented here reached a sensitivity of 96% and a specificity of 90%. For images of high difficulty, the high false positive result was an undesirable outcome, however the results in this group exceeded expectations.

A major issue with quantitative and computational medical tasks that are reported in the literature is that, without a thorough and sensible performance evaluation, metrics for performance can be almost impossible to interpret. There must be a meaningful interpretation of such algorithms such that the reader understands its usefulness in a clinical setting. We have presented a meaningful performance evaluation, whereby we stratify performance metrics with respect to the difficulty of the tasks, as well as disease characteristics which are known to impact detectability i.e., location, collateral flow. Therefore, we propose that these results represent what can be expected from real clinical implantation with naturally occurring patient variability and input scan quality variability. Referring to [Table 4](#), there is variation in the prevalence of M2 occlusions between this study and the entire INSPIRE registry, however occlusions in large distal M2 segments can simulate an M1 occlusion, and vice versa, making the actual prevalence of M2 occlusions subject to debate [\[20,21\]](#). Indeed, some estimate that M2 occlusions number as many as half the number of M1 occlusions [\[22\]](#), as is the case in this study where the data was annotated by a team of stroke experts.

The high sensitivity for M2 occlusions has not previously been reported, or patients with an M2 occlusion excluded due to the distal nature of the occlusion making it challenging to automatically detect. A significant portion of our data are patients with M2 occlusions and we consider the sensitivity (81%) of the algorithm towards M2 occlusions a significant result.

We have also investigated the benefits of including perfusion data in the model. When perfusion data was made available, it was used to provide evidence of occlusion presence. While it is an impressive feat to detect on one data type alone, all available data should be integrated into computational tools to produce the best possible result for the patient. By presenting this study, clinicians know what to expect when perfusion data is not used.

Performance was also evaluated over separate sites, with a significant drop in performance for Site 2 (e.g. 77% sensitivity, down from 89%). This demonstrates that performance can be expected to vary across sites, even with the same scanner make and model, possibly due to the differences in acquisition. Future studies will include data from more sites and scanner types.

There were some limitations to this study. First, the algorithm required pre-registered data. Due to the probabilistic nature of the registration process, there may be slight variation to the image with each attempt at registration. However, applying spatial normalization is

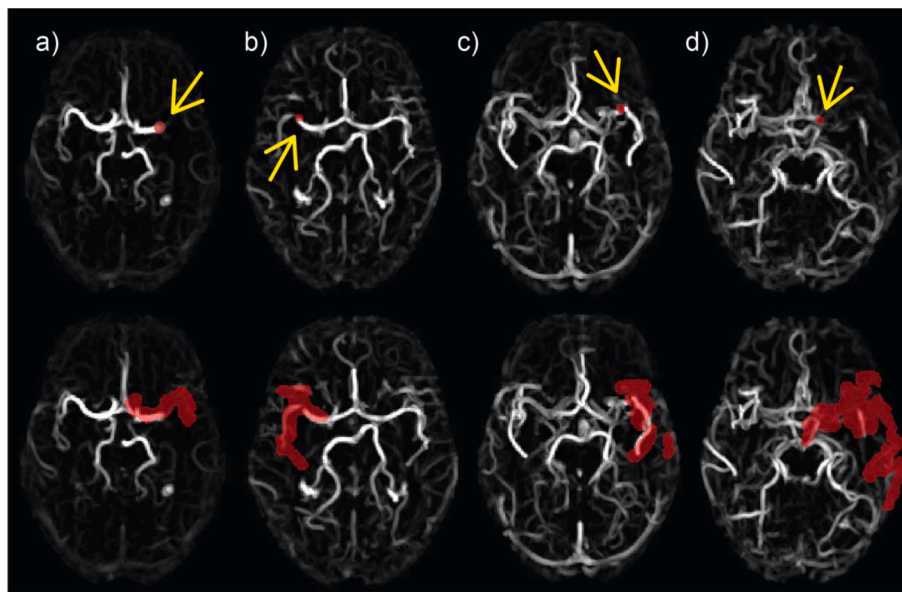


**Fig. 4.** Successful occlusion detections. The ground truth locations of each occlusion are indicated with the yellow arrow on the top row. The bottom row shows the results of the algorithm, returning regions (red) based on lack of contrast in vessel structures. Images of low (a), moderate (b) and high (c) difficulty are represented. In d) an ICA occlusion returned a large area, covering both the occlusion and contrast deficit.

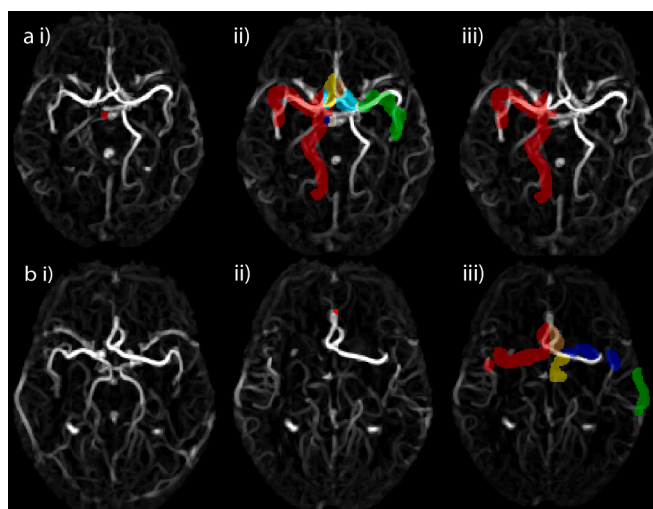


**Fig. 5.** Occlusions close to the midline. a) A basilar occlusion. (i) the ground truth annotation is shown on an axial slice of the sliding MIP; (ii) all seeds for potential occlusion locations; (iii) seed chosen as site of contrast deficit associated with the occlusion. This case is marked as a True Positive. Note the right M1 branch of the Middle Cerebral Artery (MCA) is highlighted due to natural vessel variation and was joined to the deficit region due to its close proximity, as in Fig. 2; b) An anterior cerebral artery (ACA) occlusion. (i) Axial slice showing MCA territory; (ii) axial slices showing the ground truth annotation; (iii) all seeds for potential occlusion locations. Upon analysis of seeds none were selected as the location of deficit due to an occlusion. This case received a False Negative.

highly beneficial as it facilitates the use of *a priori* knowledge to provide spatial context. Second, this method used dynamic CTA (derived from CTP) rather than conventional single timepoint CTA. For this phase of development, CTP images were used, but with further development, this method may be generalised to CTA images. This will resolve difficulties relating to extracranial ICA occlusions out of the image field-of-view, as neck coverage is included in conventional CTA acquisitions for acute stroke. Third, the algorithm focused on lack of contrast and a left–right comparison to exploit the symmetry of the brain. A healthy subject may

have returned a false positive result due to natural variation from one hemisphere to another. Due to this, the difference map (see Section 2.4) may return healthy areas that are inherited by the seeds (see Fig. 2 and Fig. 5; in the latter the PCA is highlighted along with the M1-MCA, in the latter the M1-MCA is highlighted together with the basilar territory). Hard-cut offs were used to reduce false positives, but these resulted in difficulties detecting some cases, such as those lying on the midline (Fig. 52 and Fig B1). Additional solutions were employed to manage natural variations between hemisphere and details on this can be found in the appendices. Further developments are planned that will replace hard cut-offs with more robust solutions that do not exclude occlusions lying on the midline and vessel with regular hemispheric variation. Deep Learning methods may improve on the algorithms ability to identify healthy vessels when they are not symmetrical and are being currently investigated as an alternative.

Further testing is required to optimized and justify each element in the algorithm pipeline. At this stage, performance was evaluated qualitatively, and reviewed carefully by two or more experts. This was an in-depth and lengthy process but ensured that results are reliable. Developing a robust computational method for evaluation will allow for study into each component of the pipeline. However, any automated evaluation will have to be thoroughly evaluated before it can be represented as an accurate metric of performance. A method is currently in development. Further studies investigating the implementation of the algorithms in a clinical setting and their impact on clinical workflows are required. In particular, the application of this algorithm in the context of multimodal Flat-detector CT (FD-CT) is a worthy future development. By using FD-CT as a one-stop-shop for stroke diagnosis, treatment can be expedited. The benefit of algorithmic assistance in this context should be investigated.

## 5. Conclusion

In summary, our method for automated occlusion detection in dynamic CTA images is highly sensitive. We found that specificity is improved by using perfusion data where it is available. Compared to other studies, we have presented a cohort with a large variety of occlusions in terms of location and significance. We have reviewed the performance of our algorithm in a thorough manner, including judging the performance of the algorithm with respect to the difficulty of the

**Table 2**

Table of results when perfusion data was available. The number in each group is included (N). Metrics included are sensitivity, specificity, positive predictive value (PPV), negative predictive value (NPV), diagnostic odds ratio (DOR) and Accuracy. 95% Confidence interval are added where it was calculated, in square brackets.

	N	Sensitivity	Specificity	PPV	NPV	DOR	Accuracy
All cases	205	0.83 [0.74–0.95]	0.58 [0.49–0.85]	0.83 [0.73–0.95]	0.58 [0.37–0.85]	7.06	0.76 [0.66–0.86]
Low difficulty	106	0.96	0.9	0.96	0.9	21.9	0.94
Mod. difficulty	45	0.88	0.50	0.83	0.5	7.25	0.78
High difficulty	56	0.53	0.11	0.54	0.11	0.14	0.39
IC-ICA	8	1	0.81	0.5	0.81	inf	0.84
MCA-M1	83	0.94	0.80	0.89	0.8	59.11	0.89
MCA-M2	48	0.81	0.65	0.6	0.65	7.63	0.71
MCA-M3	7	0.6	0.78	0.23	0.78	5.25	0.76
Good Collaterals	43	0.78	0.76	0.74	0.76	10.96	0.77
Poor Collaterals	48	0.95	0.73	0.75	0.73	53.85	0.83

**Table 3**

Table of results when perfusion data was not available. The number in each group is included (N). Metrics included are sensitivity, specificity, positive predictive value (PPV), negative predictive value (NPV), diagnostic odds ratio (DOR) and Accuracy. 95% Confidence interval are added where it was calculated, in square brackets.

	N	Sensitivity	Specificity	PPV	NPV	DOR	Accuracy
All	205	0.91 [0.84–1.00]	0.2 [0.14–0.35]	0.66 [0.55–0.79]	0.2 [0.05–0.35]	2.46	0.65 [0.54–0.78]
Low difficulty	106	0.97	0.41	0.79	0.41	24.63	0.8
Mod. difficulty	45	0.96	0.06	0.63	0.06	1.69	0.62
High difficulty	56	0.68	0.04	0.43	0.04	0.08	0.37
IC-ICA	8	1	0.35	0.22	0.35	inf	0.45
MCA-M1	83	0.96	0.32	0.7	0.32	11.72	0.72
MCA-M2	48	0.96	0.24	0.36	0.24	8.62	0.47
MCA-M3	7	0.6	0.33	0.09	0.33	0.75	0.36
Good Collaterals	43	0.82	0.31	0.48	0.31	2.01	0.53
Poor Collaterals	48	1	0.3	0.53	0.3	inf	0.61

**Table 4**

The prevalence of occlusion locations in this study as compared with the INSPIRE population.

Occlusion Location	Study prevalence (%) n = 207	INSPIRE prevalence (%) n = 3063
IC-ICA	4	18
MCA-M1	41	41
MCA-M2	24	12
MCA-M3	4	3
ACA	2	1.9
PCA	4	3.1
Basilar	3	0.8
No Visible Occlusion	22	15

task. In doing so, we have provided an unbiased, real-world interpretation of algorithm performance that should generalise to a clinical setting. Further developments include generalising to conventional CTA and developing automated performance evaluation for future studies.

#### Declaration of Competing Interest

The authors declare that they have no known competing financial interests or personal relationships that could have appeared to influence the work reported in this paper.

#### Acknowledgements

We acknowledge the contribution of Professor Leonid Churilov towards the statistical analysis performed in this study.

#### Appendix A. Supplementary material

Supplementary data to this article can be found online at <https://doi.org/10.1016/j.ejrad.2023.110845>.

#### References

- [1] A. Bivard, N. Spratt, F. Miteff, C. Levi, M.W. Parsons, Tissue Is More Important than Time in Stroke Patients Being Assessed for Thrombolysis, *Front. Neurol.* 9 (2018) 41, <https://doi.org/10.3389/fneur.2018.00041>.
- [2] G.W. Albers, M. Goyal, R. Jahan, A. Bonafe, H.-C. Diener, E.I. Levy, V.M. Pereira, C. Cognard, D.J. Cohen, W. Hacke, O. Jansen, T.G. Jovin, H.P. Mattle, R. Nogueira, A.H. Siddiqui, D.R. Yavagal, B.W. Baxter, T.G. Devlin, D.K. Lopes, V. K. Reddy, R.d.M. de Rochemont, O.C. Singer, R. Bammer, J.L. Saver, Ischemic core and hypoperfusion volumes predict infarct size in SWIFT PRIME: CT Perfusion Volumes, *Ann. Neurol.* 79 (1) (2016) 76–89.
- [3] A. Bivard, C. Levi, V. Krishnamurthy, P. McElduff, F. Miteff, N.J. Spratt, G. Bateman, G. Donnan, S. Davis, M. Parsons, Perfusion computed tomography to assist decision making for stroke thrombolysis, *Brain.* 138 (2015) 1919–1931, <https://doi.org/10.1093/brain/awv071>.
- [4] B.C.V. Campbell, P.J. Mitchell, T.J. Kleinig, H.M. Dewey, L. Churilov, N. Yassi, B. Yan, R.J. Dowling, M.W. Parsons, T.J. Oxley, T.Y. Wu, M. Brooks, M.A. Simpson, F. Miteff, C.R. Levi, M. Krause, T.J. Harrington, K.C. Faulder, B.S. Steinfort, M. Priglinger, T. Ang, R. Scroop, P.A. Barber, B. McGuinness, T. Wijeratne, T. G. Phan, W. Chong, R.V. Chandra, C.F. Bladin, M. Badve, H. Rice, L. de Villiers, H. Ma, P.M. Desmond, G.A. Donnan, S.M. Davis, Endovascular Therapy for Ischemic Stroke with Perfusion-Imaging Selection, *N. Engl. J. Med.* 372 (2015) 1009–1018, <https://doi.org/10.1056/NEJMoa1414792>.
- [5] B.C.V. Campbell, S. Christensen, C.R. Levi, P.M. Desmond, G.A. Donnan, S. M. Davis, M.W. Parsons, Cerebral Blood Flow Is the Optimal CT Perfusion Parameter for Assessing Infarct Core, *Stroke.* 42 (2011) 3435–3440, <https://doi.org/10.1161/STROKEAHA.111.618355>.
- [6] G.W. Albers, M.P. Marks, S. Kemp, S. Christensen, J.P. Tsai, S. Ortega-Gutierrez, R. A. McTaggart, M.T. Torbey, M. Kim-Tenser, T. Leslie-Mazwi, A. Sarraj, S.E. Kasner, S.A. Ansari, S.D. Yeatts, S. Hamilton, M. Mlynash, J.J. Heit, G. Zaharchuk, S. Kim, J. Carrozella, Y.Y. Palesch, A.M. Demchuk, R. Bammer, P.W. Lavori, J. P. Broderick, M.G. Lansberg, Thrombectomy for Stroke at 6 to 16 Hours with Selection by Perfusion Imaging, *N. Engl. J. Med.* 378 (2018) 708–718, <https://doi.org/10.1056/NEJMoa1713973>.
- [7] B.C.V. Campbell, H. Ma, P.A. Ringleb, M.W. Parsons, L. Churilov, M. Bendszus, C. R. Levi, C. Hsu, T.J. Kleinig, M. Fatar, D. Leys, C. Molina, T. Wijeratne, S. Curtze, H. M. Dewey, P.A. Barber, K.S. Butcher, D.A. De Silva, C.F. Bladin, N. Yassi, J.A. R. Pfaff, G. Sharma, A. Bivard, P.M. Desmond, S. Schwab, P.D. Schellinger, B. Yan, P.J. Mitchell, J. Serena, D. Toni, V. Thijs, W. Hacke, S.M. Davis, G.A. Donnan, G. A. Donnan, S.M. Davis, H. Ma, B.C.V. Campbell, L. Churilov, M.W. Parsons, B. Yan, P.J. Mitchell, N. Yassi, G. Sharma, P.M. Desmond, T. Oxley, T.Y. Wu, D. Shah, H. Zhao, E. Rodrigues, P. Salvaris, F. Alemseged, F. Ng, C. Williams, J.-L. Ng, H.-T.-H. Tu, A. McDonald, D. Jackson, J. Tsoleridis, R. McCoy, L. Pesavento, L. Weir, A. Bivard, T.J. Kleinig, S. Patel, J. Harvey, J. Mahadevan, E. Cheong, A. Balabanski, M. Waters, R. Drew, J. Craneffeld, T. Wijeratne, E. Mackey, S. Celestino, E. Low, H. M. Dewey, C.F. Bladin, P.S. Loh, P.M. Choi, S. Coote, T. Frost, K. Hogan, C. Ding, S. McModie, W.W. Zhang, C. Kyndt, A. Moore, Z. Ross, J. Liu, F. Miteff, C.R. Levi,

- T. Ang, N. Spratt, C. Garcia-Esperon, L. Kaauwai, T.G. Phan, J. Ly, S. Singhal, B. Clissold, K. Wong, M. Krause, S. Day, J. Sturm, B. O'Brian, R. Grimley, V. Thijs, M. Simpson, M. Lee-Archer, A. Brodtmann, B. Coulton, D. Young, A.A. Wong, C. Muller, D.K. Field, W. Vallat, V. Maxwell, P. Bailey, A. Sabet, S. Mishra, M. Tan, K. George, P.A. Barber, L. Zhao, A. Meretoja, S. Curtze, T. Tatlisumak, G. Sibolt, M. Tiainen, M. Koivu, K. Aarnio, J. Virta, O. Kasari, S. Eirola, M.C. Sun, T.C. Chen, C.S. Chuang, Y.Y. Chen, C.M. Lin, S.C. Ho, P.M. Hsiao, C.H. Tsai, W.S. Huang, Y. W. Yang, H.Y. Huang, W.C. Wang, C.H. Liu, M.K. Lu, C.H. Lu, W.L. Kung, S. K. Jiang, Y.H. Wu, S.C. Huang, C.H. Tseng, L.T. Tseng, Y.C. Guo, D. Lin, C.T. Hsu, C.W. Kuan, J.P. Hsu, H.T. Tsai, M. Suzuki, Y. Sun, H.F. Chen, C.J. Lu, C.H. Lin, C. C. Huang, H.J. Chu, C.Y. Lee, W.H. Chang, Y.C. Lo, Y.T. Hsu, C.H. Chen, P.S. Sung, C.L. Ysai, J.S. Jeng, S.C. Tang, L.K. Tsai, S.J. Yeh, Y.C. Lee, Y.T. Wang, T.C. Chung, C.J. Hu, L. Chan, Y.W. Chiou, L.M. Lien, H.L. Yeh, J.H. Yeh, W.H. Chen, C.L. Lau, A. Chang, I.Y. Lee, M.Y. Huang, J.T. Lee, G.S. Peng, J.C. Lim, Y.D. Hsu, C.C. Lin, C. A. Cheng, C.H. Yen, F.C. Yang, C.H. Hsu, Y.F. Sung, C.K. Tsai, C.L. Tsai, P.M. Hsiao, A. Lee, G. Hankey, D. Blacker, R. Gerraty, C.-I. Chen, C.-S. Hsu, E. Cowley, R. McCoy, M. Sallaberger, B. Snow, J. Kolbe, R. Stark, J. King, R. Macdonnell, J. Attia, C. D'Este, J. Bernhardt, L. Carey, D. Cadilhac, C. Anderson, D. Howells, A. Barber, A. Connelly, M. Macleod, V. O'Collins, W. Wilson, L. Macaulay, M. Bendszus, E. Bluhmki, C. Eschenfelder, W. Hacke, C. Molina, D. Leys, P. Ringleb, P. Schellinger, S. Schwab, D. Toni, N. Wahlgren, J. Wardlaw, C. Oppenheim, K. R. Lees, M. Kaste, R. von Kummer, G. Chatellier, R. Laage, X. Nunez, C. Ehrenkrona, A.-S. Svenson, L. Cove, K. Niederkorn, F. Gruber, P. Kapeller, R. Mikulik, J.-L. Mas, J. Berrouschot, J. Sobesky, M. Köhrmann, T. Steiner, C. Kessler, M. Fatar, R. Dziewas, S. Poli, K. Althaus-Knaurer, P. Bovi, A. L. Rodriguez, J.F. Arenillas, K. Muir, R. Veltkamp, A. Dixit, G. Muddegowda, L. Kala, D.A. De Silva, K.S. Butcher, G. Byrnes, A. Peeters, J.B. Chalk, J.N. Fink, T. E. Kimber, D. Schultz, P.J. Hand, J. Frayne, B.M. Tress, J. McNeil, R. Burns, C. Johnston, M. Williams, Extending thrombolysis to 4-5-9 h and wake-up stroke using perfusion imaging: a systematic review and meta-analysis of individual patient data, *The Lancet*. 394 (2019) 139-147, [https://doi.org/10.1016/S0140-6736\(19\)31053-0](https://doi.org/10.1016/S0140-6736(19)31053-0).
- [8] R.G. Nogueira, A.P. Jadhav, D.C. Haussen, A. Bonafe, R.F. Budzik, P. Bhuva, D. R. Yavagal, M. Ribo, C. Cognard, R.A. Hanel, C.A. Sila, A.E. Hassan, M. Millan, E. I. Levy, P. Mitchell, M. Chen, J.D. English, Q.A. Shah, F.L. Silver, V.M. Pereira, B. P. Mehta, B.W. Baxter, M.G. Abraham, P. Cardona, E. Veznedaroglu, F.R. Hellinger, L. Feng, J.F. Kirmani, D.K. Lopes, B.T. Jankowitz, M.R. Frankel, V. Costalat, N. A. Vora, A.J. Yoo, A.M. Malik, A.J. Furlan, M. Rubiera, A. Aghaebrahim, J.-M. Olivot, W.G. Tekle, R. Shields, T. Graves, R.J. Lewis, W.S. Smith, D. S. Liebeskind, J.L. Saver, T.G. Jovin, Thrombectomy 6 to 24 Hours after Stroke with a Mismatch between Deficit and Infarct, *N. Engl. J. Med.* 378 (2018) 11-21, <https://doi.org/10.1056/NEJMoal706442>.
- [9] S. Dehkharghani, M. Lansberg, C. Venkatsubramanian, C. Cereda, F. Lima, H. Coelho, F. Rocha, A. Qureshi, H. Haerian, F. Mont'Alverne, K. Copeland, J. Heit, High-Performance Automated Anterior Circulation CT Angiographic Clot Detection in Acute Stroke: A Multireader Comparison, *Radiology*. 298 (3) (2021) 665-670.
- [10] S.P.R. Luijten, L. Wolff, M.H.C. Duvekot, P.-J. van Doormaal, W. Moudroux, H. Kerkhoff, G.J. Lycklama a Nijeholt, R.P.H. Bokkers, L.S.F. Yo, J. Hofmeijer, W. H. van Zwam, A.C.G.M. van Es, D.W.J. Dippel, B. Roozenbeek, A. van der Lugt, van der Lugt, Diagnostic performance of an algorithm for automated large vessel occlusion detection on CT angiography, *J. NeuroInterventional Surg.* 14 (8) (2022) 794-798.
- [11] T. Dobrocky, E.I. Piechowiak, B. Volbers, N. Slavova, J. Kaesmacher, T.R. Meinert, M. Arnold, U. Fischer, S. Jung, J. Gralla, P. Mordasini, M.R. Heldner, Treatment and Outcome in Stroke Patients With Acute M2 Occlusion and Minor Neurological Deficits, *Stroke*. 52 (2021) 802-810, <https://doi.org/10.1161/STROKEAHA.120.031672>.
- [12] F.O. Lima, K.L. Furie, G.S. Silva, M.H. Lev, É.C.S. Camargo, A.B. Singhal, G. J. Harris, E.F. Halpern, W.J. Koroshetz, W.S. Smith, R.G. Nogueira, Prognosis of Untreated Strokes Due to Anterior Circulation Proximal Intracranial Arterial Occlusions Detected by Use of Computed Tomography Angiography, *JAMA Neurol.* 71 (2014) 151, <https://doi.org/10.1001/jamaneurol.2013.5007>.
- [13] O. Volny, P. Cimflova, P. Kadlecova, P. Vanek, J. Vanicek, B.K. Menon, R. Mikulik, Single-Phase Versus Multiphase CT Angiography in Middle Cerebral Artery Clot Detection—Benefits for Less Experienced Radiologists and Neurologists, *J. Stroke Cerebrovasc. Dis.* 26 (2017) 19-24, <https://doi.org/10.1016/j.jstrokecerebrovasdis.2016.08.023>.
- [14] F. Tang, D.K.S. Ng, D.H.K. Chow, An image feature approach for computer-aided detection of ischemic stroke, *Comput. Biol. Med.* 41 (2011) 529-536, <https://doi.org/10.1016/j.combiomed.2011.05.001>.
- [15] B.K. Menon, F.S. Al-Ajlan, M. Najm, J. Puig, M. Castellanos, D. Dowlatabadi, A. Calleja, S.-I. Sohn, S.H. Ahn, A. Poppe, R. Mikulik, N. Asdaghi, T.S. Field, A. Jin, T. Asil, J.-M. Boulanger, E.E. Smith, S.B. Coutts, P.A. Barber, S. Bal, S. Subramanian, S. Mishra, A. Trivedi, S. Dey, M. Eesa, T. Sajobi, M. Goyal, M. D. Hill, A.M. Demchuk, for the INTERSECT Study Investigators, Association of Clinical, Imaging, and Thrombus Characteristics With Recanalization of Visible Intracranial Occlusion in Patients With Acute Ischemic Stroke, *JAMA*. 320 (10) (2018) 1017.
- [16] P.A. Yushkevich, J. Piven, H.C. Hazlett, R.G. Smith, S. Ho, J.C. Gee, G. Gerig, User-guided 3D active contour segmentation of anatomical structures: Significantly improved efficiency and reliability, *NeuroImage*. 31 (2006) 1116-1128, <https://doi.org/10.1016/j.neuroimage.2006.01.015>.
- [17] B. Avants, N.J. Tustison, G. Song, Advanced Normalization Tools: V1.0, *Insight J.* (2009), <https://doi.org/10.54294/uvninh>.
- [18] C. Rorden, L. Bonilha, J. Fridriksson, B. Bender, H.-O. Karnath, Age-specific CT and MRI templates for spatial normalization, *NeuroImage*. 61 (2012) 957-965, <https://doi.org/10.1016/j.neuroimage.2012.03.020>.
- [19] M. McCormick, X. Liu, J. Jomier, C. Marion, L. Ibanez, ITK: enabling reproducible research and open science, *Front. Neuroinformatics*. 8 (2014), <https://doi.org/10.3389/fninf.2014.00013>.
- [20] G. Duloquin, M. Graber, L. Garnier, V. Crespy, P.-O. Comby, L. Baptiste, S. Mohr, B. Delpont, J. Guéniat, C. Blanc-Labarre, M. Hervieu-Bègue, G.-V. Osseby, M. Giroud, Y. Béjat, Incidence of Acute Ischemic Stroke With Visible Arterial Occlusion: A Population-Based Study (Dijon Stroke Registry), *Stroke*. 51 (2020) 2122-2130, <https://doi.org/10.1161/STROKEAHA.120.029949>.
- [21] A. Żytkowski, E. Clarke, A. Olszewska, A. Mazurek, A. Dubrowski, M. Radek, Early bifurcation of the middle cerebral artery – A case report with commentaries on the clinical significance, *Transl. Res. Anat.* 26 (2022), 100161, <https://doi.org/10.1016/j.tria.2022.100161>.
- [22] A.T. Rai, J.R. Domico, C. Buseman, A.R. Tarabishy, D. Fulks, N. Lucke-Wold, S. Boo, J.S. Carpenter, A population-based incidence of M2 strokes indicates potential expansion of large vessel occlusions amenable to endovascular therapy, *J. NeuroInterventional Surg.* 10 (2018) 510-515, <https://doi.org/10.1136/neurintsurg-2017-013371>.